Unraveling the spin current flow in Bi layers

Kacio Mello,[1] José E. Abrão ⬤,[1] Eduardo S. Santos ⬤,[1] Joaquim B. S. Mendes,[2]
Ernesto P. Raposo,[3] and Antonio Azevedo ⬤[1,*]

[1]*Departamento de Física, Universidade Federal de Pernambuco, Recife, Pernambuco 50670-901, Brazil*
[2]*Departamento de Física, Universidade Federal de Viçosa, 36570-900 Viçosa, Minas Gerais, Brazil*
[3]*Laboratório de Física Teórica e Computacional, Departamento de Física,*
Universidade Federal de Pernambuco, Recife, Pernambuco 50670-901, Brazil

Although heavy metal materials, due to their large spin-orbit interaction, would be expected to act as an efficient converter of spin current to charge current, Bismuth does not obey this rule. Heterostructures of yttrium iron garnet (YIG)/Bi are investigated by means of the spin pumping technique and the results show that Bi exhibits negligible spin-charge conversion. In addition to not converting spin to charge, Bi exhibits an exotic spin relaxation mechanism, which is driven by its large diamagnetic response. By considering a nonlinear stochastic model of diffusing spin particles, the results show that the Bi layer acts as a binary classifier device that categorizes the pumped spins into relaxed spins and those that flow upwards and eventually reach the top layer of Pt. This shows that the investigation reported here opens different perspectives involving fundamental aspects in the fields of machine learning and condensed matter physics.

I. INTRODUCTION

Large spin-orbit coupling (SOC) is known to be one of the key requirements for a material to be an efficient spin-to-charge current converter. In addition, it has been also well established [1] that the strength of the SOC rapidly increases with the atomic number, and among the materials with large SOC bismuth (Bi) is recognized as the heaviest nonradioactive chemical element, with $Z = 83$. Therefore, Bi should be a fundamental material for investigations on the spin-to-charge current conversion because of its strong SOC of the order of 1.5 eV [2–5]. Besides having a strong SOC, Bi is also an element usually present in several topological insulator (TI) compounds, such as $Bi_{1-x}Sb_x$, Bi_2Se_3, Bi_2Te_3, and $MnBi_2Te_4$, and it is known as well that Bi itself is considered a topological material [2,5–16]. Among the elemental materials, Bi exhibits a number of remarkable properties, namely (i) it is the one with largest diamagnetism, (ii) highest thermoelectric coefficient, (iii) highest Hall coefficient, and (iv) highest magnetoresistance, among other notable features [17]. Therefore, the investigation of the materials properties of Bi is of extreme importance nowadays.

Several previous works have reported the experimental detection of spin-to-charge mutual conversion not only in the bulk of Bi but also at Bi/Ag interfaces [18–20]. However, a recent work [5] has proposed that Bi should exhibit negligible spin-to-charge interconversion properties based on the investigation of spin current injection by means of the spin Seebeck effect (SSE) in FI/Bi/HM structures, where FI is the ferrimagnetic insulator $Y_3Fe_5O_{12}$ (YIG) and HM is a heavy metal such as Pt or W. The main reason for the controversial measurements of mutual conversion between charge and spin currents is probably related to the use of ferromagnetic metal (FM) layers as the spin injector into the Bi layer. If the microwave-driven spin pumping (SP) or thermal-driven longitudinal spin Seebeck effect (LSSE) techniques are employed to investigate the spin-to-charge current conversion in FM/HM bilayers, there arise spurious contributions to the signal that should be taken into account. For example, Permalloy ($Py = Ni_{81}Fe_{19}$) films under ferromagnetic resonance (FMR) generate a self-induced spin-charge conversion that overlaps the charge current generated by the inverse spin Hall effect (ISHE), thus hampering the analysis of the ISHE voltage signal in Py/HM bilayers [21,22]. Also, when a Py/HM bilayer is submitted to an out-of-plane temperature gradient ($\nabla_z T$), it injects a perpendicular spin current $j_S \parallel \nabla_z T$ from the Py into the HM due to the LSSE, which gives rise to an electric field $E_{ISHE} \propto (j_S \times \sigma)$ along the HM plane, where $\sigma \parallel \mathbf{M}_{Py}$.

Superimposed to this ISHE field, there also appear additional electric fields due to two thermoelectric effects, namely the ordinary Nernst effect (ONE) [23] and the anomalous Nernst effect (ANE) [24]. In the ONE, which is the counterpart of the ordinary Hall effect, a transverse electric field (E_{ONE}) is generated perpendicular to both the temperature gradient (∇T) and applied magnetic field (B), where $E_{ONE} \propto \nabla T \times B$. On the other hand, in the ANE, which is the counterpart of the anomalous Hall effect, a transverse electric field (E_{ANE}) is generated perpendicular to both ∇T and magnetization (M), where $E_{ANE} \propto \nabla T \times M$. Contrary to the ONE, the ANE rapidly increases in low magnetic fields. We remark that E_{ISHE} is created in the HM only, E_{ONE} is created in both the FM and HM, and E_{ANE} is created in the FM (metal).

*antonio.azevedo@ufpe.br

Moreover, in any thermally driven SP experiment on metals or semiconductors, the ordinary Seebeck effect (OSE) has to be taken into account. The OSE gives rise to an electromotive force parallel to ∇T, which does not depend on the applied magnetic field and can be significant in materials with large Seebeck coefficient, such as Bi. All these effects will overlap, making it difficult to analyze the resulting signal in FM/HM (metallic bilayers) under a temperature gradient [25]. The use of a FI as pure spin current generator eliminates [5] most of the aforementioned difficulties introduced when FMs are employed as spin injectors [26,27]. For example, in YIG/HM bilayer structures the contributions from ANE and ONE are excluded from the YIG, meaning that the only contributions to the voltage arises from the ONE, ISHE, and OSE generated in the HM layer. As we shall present below, YIG/Bi bilayers are very peculiar systems in which the spin-to-charge conversion is negligible and only a spurious contribution due to OSE exists.

II. RESULTS

A reliable technique that can certainly shed light on the controversy of the spin-charge conversion in Bi is the SP technique, in which the FMR of the FI in the FI/Bi bilayers is excited. As the magnetization precesses, it injects a pure spin current (j_S) across the FI/Bi interface that, as theoretically expected, should be converted into a transverse charge current (j_C) by means of the ISHE, and can be, in principle, detected by measuring an ISHE voltage between two electrodes attached to the HM layer. Albeit the use of FI as spin injectors eliminates spurious effects due to the charge carriers, it is still possible to have contributions from thermal effects that eventually occur due to the small heating of the FI layer under FMR, as discussed below. In this context, it is quite important to emphasize that the charge current generated by the ISHE must satisfy the equation $j_C = (2e/\hbar)\theta_{SH}(j_S \times \sigma)$, where σ is the spin polarization, θ_{SH} is the spin Hall angle, and e and $\hbar$ are the electron charge and reduced Planck constant, respectively. If the voltage cannot be explained by this equation, it means that the signal is contaminated by spurious effects generated by phenomena other than the spin-charge conversion.

In this work, we investigate the spin-charge conversion in YIG(40 nm)/Bi and YIG(40 nm)/Bi (0–10 nm)/HM(6 nm) heterostructures, where HM = Pt or W, by means of the microwave-driven SP technique. Fig. 1(a) schematically shows the FMR-driven SP technique and Fig. 1(b) [top (black), middle (red), and bottom (blue)] displays the field scan FMR absorption curves for pure YIG, YIG/Bi, and YIG/Pt, respectively. It is important to note the increase in the FMR linewidth of the YIG/HM bilayers due to the spin angular moment transfer to the adjacent metal layer. Experimental details as well as the sample characterization are available in the Supplemental Material [28] (see also Ref. [18] there in).

Figures 1(c)–1(e) show the SP current I_{SP} ($I_{SP} = V_{SP}/R$, where R is the electrical resistance between the electrodes) obtained in a YIG/Bi(8 nm) bilayer as function of the rf power, for three different angular positions $\phi = 0°$, $90°$, $180°$, with ϕ defined in the inset of Fig. 1(c). The inset of Fig. 1(d) shows typical spin pumping current (I_{SP}) signals obtained in a YIG/Pt(6 nm) bilayer, which exactly obey the equation

$j_C = (2e/\hbar)\theta_{SH}(j_S \times \sigma)$, i.e., null at $\phi = 90°$ (black), maximum positive at $\phi = 0°$ (red), and maximum negative at $\phi = 180°$ (blue). The I_{SP} signals displayed in Figs. 1(c)–1(e) do exhibit a behavior completely different from that of the I_{SP} signal generated by the YIG/Pt bilayer. Indeed, the I_{SP} signals do not invert the polarization for $\phi = 0°$ and $\phi = 180°$ and V_{SP} is not null at $\phi = 90°$, i.e., they do not depend on the magnetic field direction.

The origin of the electric signals shown in Figs. 1(c)–1(e), which were attributed in previous works [18–20] as due to the spin-to-charge current conversion by the ISHE, in a different context, is certainly due to the OSE. At the FMR condition, the energy absorbed by the uniform precession mode relaxes into phonons by different channels leading to sample heating [29,30]. Therefore, the YIG film heats up, generating a ∇T perpendicular to the Bi film that would hypothetically drive the ONE. Keeping the external magnetic field along the direction $\phi = 90°$, the ONE and ISHE voltages are null along this direction and maximum in the perpendicular direction, thus obeying the equations $E_{ONE} \propto \nabla T \times B$ and $E_{ISHE} \propto (j_S \times \sigma)$, respectively. As the current signals displayed in Figs. 1(c)–1(e) do not depend on the magnetic field direction, they cannot be attributed to the ONE or ISHE, but certainly can be associated with the OSE due to the small ∇T along the sample plane that is peaked up at the FMR. As Bi has the largest Seebeck coefficient, $-72 \, \mu V/K$ [31], a small in-plane ∇T gives rise to voltage values of few microvolts. Some works have recently reported further results about the thermoelectric contributions to the spin pumping signals in FM/NM bilayers [32–34], where NM = nonmagnetic metal.

The most surprising result is the nonexistence of the ISHE signal generated in the Bi layer. To investigate whether the spin current injected by SP would transmit through the Bi layer, we prepared samples of YIG/Bi(t_{Bi})/Pt(6 nm) with distinct Bi layer thicknesses, $t_{Bi} = 0, 2, 4, 6, 8$ nm. Fig. 2(a)–2(d) show clear ISHE signals measured in the top Pt layer as a function of t_{Bi}. Interestingly, the ISHE signal suddenly decreases with t_{Bi}, as shown in Fig. 2(f). For $t_{Bi} = 8$ nm the SP current signal does not reach the top layer of Pt, indicating that in addition to not converting spin current into charge current, Bi exhibits a relevant spin relaxation mechanism. In this sense, the good fit to the expression obtained from a nonlinear diffusion model of spin current flow (see below), shown in Fig. 2(f) by the solid line, can give a clue about the spin damping mechanism acting in the Bi layer.

III. THEORETICAL MODEL

As a model, we assume that the strong diamagnetism of Bi provides a relaxation channel for the pumped spin accumulation that builds up in the Bi layer due to the SP process. The applied uniform magnetic field, $H = H_0 e_x$ [see Fig. 1(a)], induces an opposite local magnetic moment in Bi, $\mu_{Bi}(r, t) = -\mu_{Bi}(r, t)e_x$, which is opposite to the magnetic moment pumped by the SP, $\mu_{SP}(r, t) = \mu_{SP}(r, t)e_x$. The interaction between the out-of-equilibrium pumped spins and the local electron spins of the Bi layer can be modeled by an effective exchange interaction given by $H_{ex} = -B_{Bi} \cdot \mu_{SP}$, where $B_{Bi}(r, t) = [2J/(g\mu_B^2)]\mu_{Bi}$ is the local effective magnetic field felt by μ_{SP}, J is the effective exchange energy,
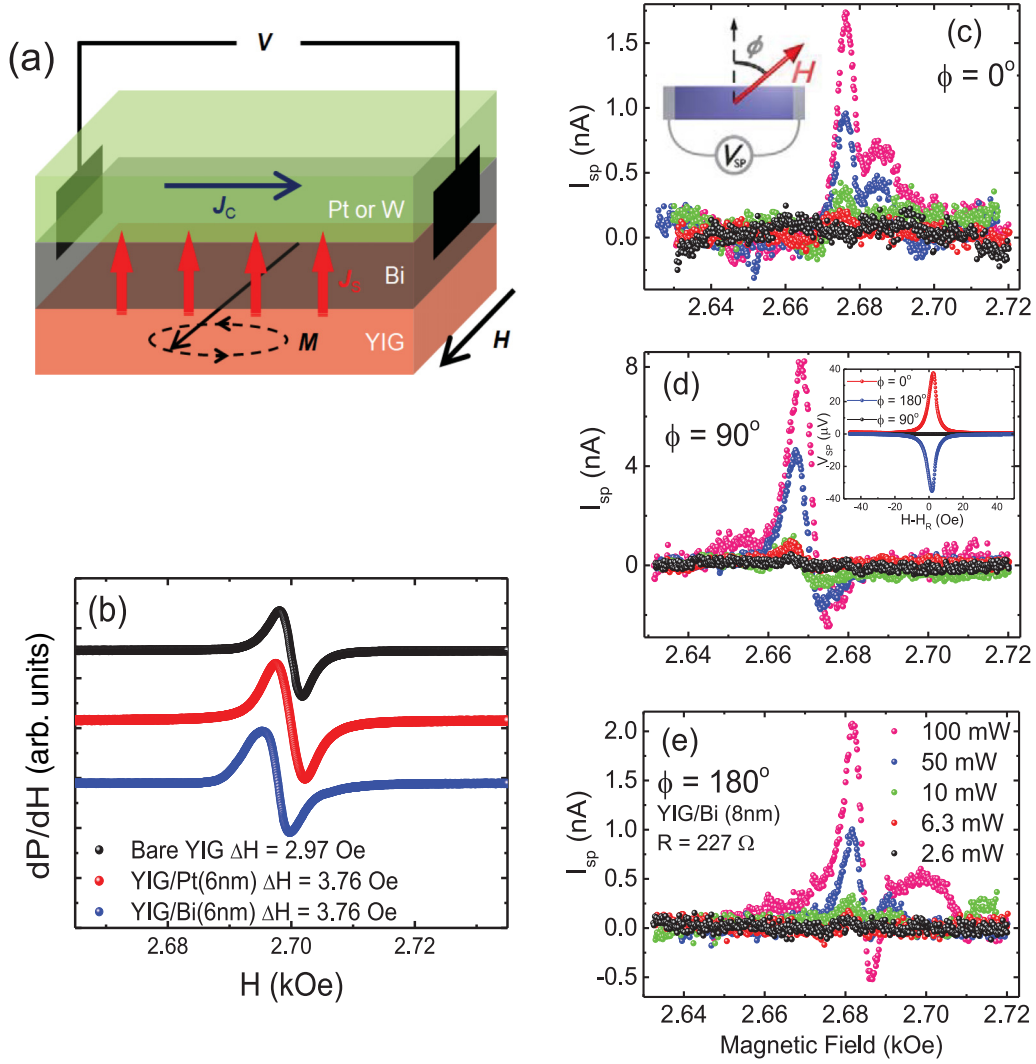
FIG. 1. (a) Schematic of the SP technique. (b) FMR field scan of pure YIG (black), YIG/Pt (red), and YIG/Bi (blue) structures. The linewidths increase due to the spin angular moment transfer from YIG to the HM layer. (c)–(e) SP current signals I_{SP} measured in YIG/Bi(8 nm) as a function of the incident rf power for three angular positions, as shown in the inset of (c). The measured SP signals cannot be explained by the equation $\boldsymbol{j}_C = (2e/\hbar)\theta_{SH}(\boldsymbol{j}_S \times \boldsymbol{\sigma})$, thus confirming that it is due to the OSE. The inset of (d) displays I_{SP} for YIG/Pt, which is exactly explained by this equation.

and g and μ_B are the Landé factor and Bohr magneton, respectively. So, as the effective local field points opposite to the external field $\boldsymbol{H}$, the induced local momenta $\boldsymbol{\mu}_{Bi}$ points antiparallel to the pumped magnetic momenta $\boldsymbol{\mu}_{SP}$. We assume as well that the conduction electrons (where the pumped spin polarization is transferred) and the localized electrons of Bi (responsible for the diamagnetic response) are separated degrees of freedom. The exchange coupling between $\boldsymbol{\mu}_{SP}$ and the diamagnetic reservoir works as a significant relaxation mechanism for the spin current. Since the pumped spin population relaxes for larger Bi layer thicknesses, the spin current reaching the upper Pt layer becomes weaker. Therefore, the dependence of the ISHE voltage at the upper Pt layer as a function of the Bi-layer thickness t_{Bi} may provide an indication for the spin current relaxation mechanism. In addition, as mentioned, temperature is also a key ingredient in the relaxation phenomenon.

The problem of a spin current flowing in a layer of a magnetic heterostructure can be addressed through diffusion models of spin particles [35–37]. To explain the t_{Bi} dependence in Fig. 2(f) of the spin current that flows in the Bi layer and eventually reaches the upper layer of Pt, we consider a modified Klein-Kramers diffusion model with nonlinear features arising from the exclusion principle. We start by denoting $(\boldsymbol{r}, \boldsymbol{p})$ as the phase space coordinates of a particle in the spin current with position $\boldsymbol{r}$, linear momentum $\boldsymbol{p}$, and spin parallel to the uniform external field. The occupation number of this coordinate at time t is $n(\boldsymbol{r}, \boldsymbol{p}, t)$. The stochastic dynamic evolution of n is driven by the master equation,

$$\frac{\partial n(\boldsymbol{r}, \boldsymbol{p}, t)}{\partial t} = \int \{\tau_{(\boldsymbol{r}', \boldsymbol{p}') \to (\boldsymbol{r}, \boldsymbol{p})} f\left(n(\boldsymbol{r}, \boldsymbol{p}, t)\right) n(\boldsymbol{r}', \boldsymbol{p}', t)$$
$$- \tau_{(\boldsymbol{r}, \boldsymbol{p}) \to (\boldsymbol{r}', \boldsymbol{p}')} f(n(\boldsymbol{r}', \boldsymbol{p}', t)) n(\boldsymbol{r}, \boldsymbol{p}, t)\} d\boldsymbol{r}' d\boldsymbol{p}',$$

(1)

where, e.g., $\tau_{(\boldsymbol{r}', \boldsymbol{p}') \to (\boldsymbol{r}, \boldsymbol{p})}$ represents the transition rate from state $(\boldsymbol{r}', \boldsymbol{p}')$ to $(\boldsymbol{r}, \boldsymbol{p})$. The function $f(n(\boldsymbol{r}, \boldsymbol{p}, t))$ is introduced to comply with the exclusion principle, i.e., $f(1) = 0$,
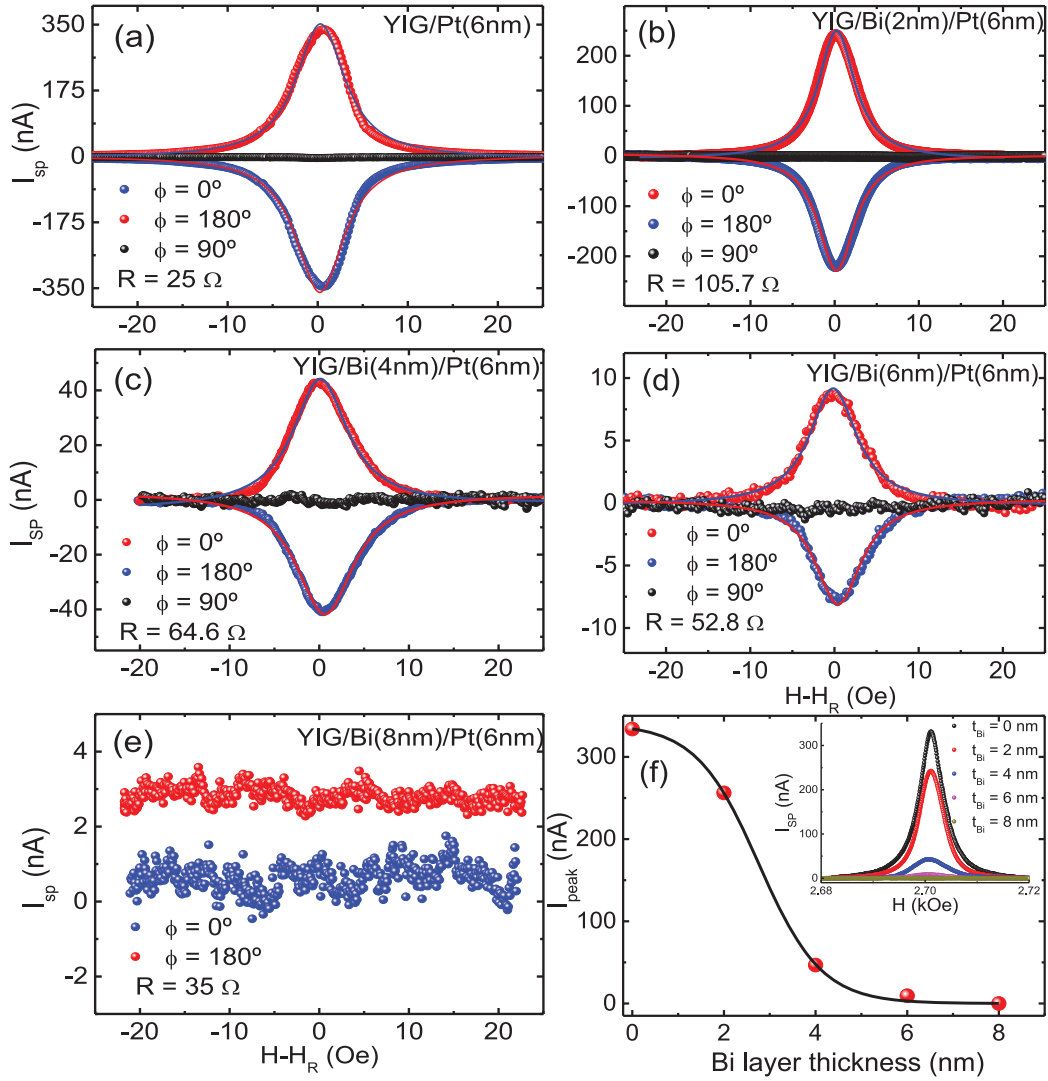
FIG. 2. Panels (a)–(f) display the SP signals measured at the top layer of Pt as a function of (a)–(e) the applied field and (f) Bi layer thickness. All absorption curves have been offset by the resonance field value H_R. Red circles in (f) display the peak value of the SP current shown in the inset as a function of t_{Bi} and the solid line is the best fit to the data using Eq. (5). The red symbols in (e) have been shifted up for better viewing.

so that the transition in time t to the arrival state $(\mathbf{r}, \mathbf{p})$ is forbidden if it is already occupied. [For spinless classical particles not subject to the exclusion principle, Eq. (1) takes the usual expression [38] with $f(n) = 1$.] We employ the form $f(n(\mathbf{r}, \mathbf{p}, t)) = 1 - n(\mathbf{r}, \mathbf{p}, t)$ considered in [39], which adds a nonlinear character to the standard linear master equation.

For the transition processes allowed in Eq. (1), the stochastic effects of thermal fluctuations are taken into account in the Langevin dynamics equation [38],

$$\frac{d\mathbf{p}}{dt} = \mathbf{F} - \eta\mathbf{p} + \alpha\boldsymbol{\xi}, \quad (2)$$

where $\mathbf{p}/m = d\mathbf{r}/dt$ and $\alpha = (2m\gamma k_B T)^{1/2}$ for a particle of mass m in a medium with absolute temperature T, damping coefficient η, and subject to a force $\mathbf{F}$ and Gaussian white noise $\boldsymbol{\xi}(t)$ with unit second-order temporal autocorrelation in each direction.

Consider now transitions between states $(\mathbf{r}', \mathbf{p}')$ to $(\mathbf{r}, \mathbf{p})$ separated in time by $dt \to 0$. For instance, $(\mathbf{r}', \mathbf{p}') =$ $(\mathbf{r}, \mathbf{p} \pm d\mathbf{p})$ represents an infinitesimal change in the particle's linear momentum due to any of the possible mechanisms described in Eq. (2) without diffusion. Conversely, $(\mathbf{r}', \mathbf{p}') = (\mathbf{r} \pm d\mathbf{r}, \mathbf{p})$ depicts a particle diffusing during dt with unchanged momentum. In this scenario the effective transition rates for changes, e.g., along the x axis are $\tau_{(x \pm dx, p_x) \to (x, p_x)} dx \sim dx/dt = p_x/m$ and $\tau_{(x, p_x \pm dp_x) \to (x, p_x)} dp_x \sim F_x - \eta p_x/2 + \alpha^2/(2dp_x)$. Simultaneous infinitesimal changes in both $\mathbf{r}'$ and $\mathbf{p}'$ as $dt \to 0$ are statistically less relevant. By combining the transition rates with Eq. (1) in the limit $dt \to 0$, $d\mathbf{r} \to 0$ and $d\mathbf{p} \to 0$, one obtains [39] the modified Klein-Kramers equation for a spin particle with potential energy $U(\mathbf{r})$ in the spin current flow,

$$\frac{\partial n(\mathbf{r}, \mathbf{p}, t)}{\partial t} = -\frac{\mathbf{p}}{m} \cdot \nabla_{\mathbf{r}}[f(n)n] + \eta\nabla_{\mathbf{p}} \cdot [\mathbf{p}f(n)n]$$

$$+ \nabla_{\mathbf{p}} \cdot [\nabla_{\mathbf{r}}U(\mathbf{r})f(n)n] + \frac{\alpha^2}{2}\nabla_{\mathbf{p}}^2 n, \quad (3)$$

which reduces to the standard Klein-Kramers equation [38] for classical spinless particles with $f(n) = 1$, as expected.

By writing the total energy of the spin particle as $E(\boldsymbol{r}, \boldsymbol{p}) = \boldsymbol{p}^2/(2m) + U(\mathbf{r})$, the stationary $[\partial n(\boldsymbol{r}, \boldsymbol{p}, t)/\partial t \to 0]$ solution of Eq. (3) in free space can be found by integration leading to the Fermi-Dirac (FD) distribution [39],

$$n(\boldsymbol{r}, \boldsymbol{p}) = \frac{1}{e^{\beta[E(\boldsymbol{r}, \boldsymbol{p}) - \mu]} + 1}, \tag{4}$$

with $\beta = (k_B T)^{-1}$ and μ as the chemical potential to fix the normalization condition of $n(\boldsymbol{r}, \boldsymbol{p})$. We can conveniently set apart in $E = E_0 + E_{\text{ex}}$ the contribution from the exchange interaction energy E_{ex} between a spin particle diffusing in the Bi layer and the antiparallel magnetic momenta of the localized electrons of Bi responsible for the diamagnetic response (the diamagnetic reservoir; see above). In a mean-field-type approximation with exchange coupling constant independent of $\boldsymbol{r}$ and fixed transverse section area of the layers, we write $E_{\text{ex}} \propto t_{\text{Bi}}$, with a positive proportionality constant due to the opposite spins of Bi and the particle in the current flow, so that the spin current reaching the Pt layer effectively reads

$$I_{\text{SP}}(t_{\text{Bi}}) = \frac{I_{\text{SP}}^*}{e^{(t_{\text{Bi}} - t_\mu)/t^*} + 1}, \tag{5}$$

where I_{SP}^* is a constant and the effective thicknesses t^* and t_μ are respectively mapped onto the temperature and chemical potential of a FD distribution. As indicated in Eq. (5), the exchange coupling between the particles in the spin current and the diamagnetic reservoir gives rise to a relevant effective relaxation of the spin current displayed in Fig. 2(f) for large Bi layer thicknesses t_{Bi}. Actually, as seen in Fig. 2(f), by setting $t^* = 0.68$ nm and $t_\mu = 2.76$ nm a nice fit to the experimental data using Eq. (5) was obtained.

IV. SPIN RELAXATION AS A BINARY CLASSIFIER

An interesting consequence of Eq. (5) is the possibility of mapping the problem of a spin current relaxing according to a FD distribution onto a binary classification problem recently reported in [40]. Binary classification is one of the key problems in machine learning research [40,41]. In this kind of problem, the response of the system is restricted to one of two possible outcomes, which are components of two disjoint sets of values. Indeed, there are only two possible outcomes at the upper Bi/Pt interface for the spin particles that are injected through the lower YIG/Bi interface. At a certain distance from the YIG/Bi interface the pumped spins will either (i) lose their polarization by relaxation or (ii) diffuse upwards to the Bi/Pt interface, eventually reaching it and being converted into a charge current in the Pt layer. As shown in Ref. [40], the FD distribution is the probabilistic output for binary classifiers in which the classification can be mapped onto the occupation number of a fermions system with appropriate effective parameters. In the present case, Fig. 3 shows the unidirectional flowchart for the binary classification process responsible for the pumped spins relaxation.

In this context, a proper question should be whether our system configuration can be controlled in some way. First, let us recall that the thermal fluctuations play a key role in the
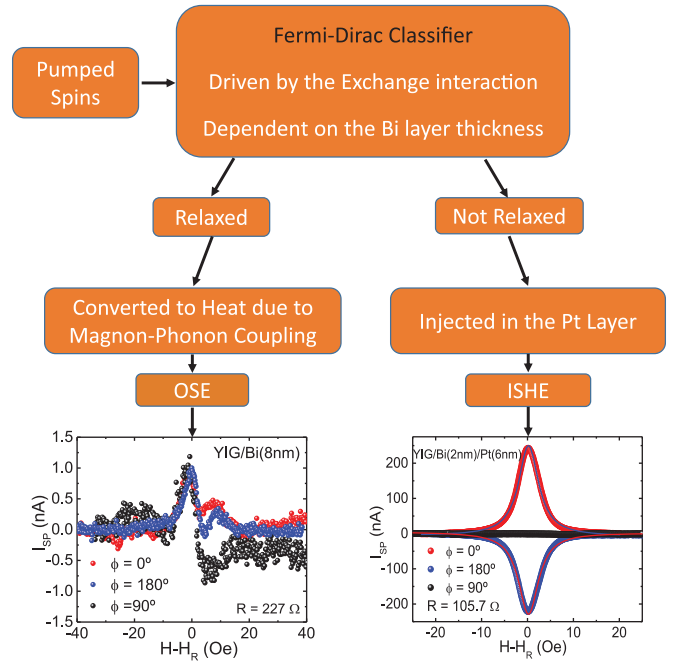

FIG. 3. Flowchart of the binary classification process in the YIG/Bi/Pt heterostructure. Spins are pumped by SP into the Bi layer and submitted to a uniform magnetic field, which generates a magnetization texture opposite to the field direction. The exchange interaction between the magnetic momenta of Bi electrons and spin particles, $\boldsymbol{\mu}_{\text{Bi}}$ and $\boldsymbol{\mu}_{\text{SP}}$, respectively, acts as a relaxation mechanism, which depends on the system temperature. For $0 < t_{\text{Bi}} < 8$ nm, part of the spins will relax to the lattice giving rise to the OSE signal, whereas the spins that do not relax will be injected through the Bi/Pt interface yielding the SP signal.

coupling between $\boldsymbol{\mu}_{\text{Bi}}$ and $\boldsymbol{\mu}_{\text{SP}}$. If the magnetic system is rigid ($T = 0$ K), there will be no applied torque ($\boldsymbol{\tau} \propto \boldsymbol{B}_{\text{Bi}} \times \boldsymbol{\mu}_{\text{SP}}$) to the pumped spins by the local effective field because they are exactly antiparallel. Considering the parameter t^* in Eq. (5) as an effective temperature, the $T = 0$ K regime would then correspond to a system configuration with $t_{\text{Bi}} = 0$, so that all pumped spins would be promptly injected into the Pt layer since the FD distribution is a step function in this case. On the other hand, if $T > 0$ K the thermal fluctuations will trigger the relaxation mechanism and this situation would be associated with a non-null Bi layer thickness in which not all injected spin particles are able to reach the Bi/Pt interface. Therefore, the value $t^* = 0.68$ nm would be effectively mapped onto the temperature of the FD classifier. The other parameter, $t_\mu = 2.76$ nm, which is related to the chemical potential, represents a threshold thickness above which most of the pumped spins are damped to the thermal bath and below which most of the pumped spins flow up to the Pt layer, being converted into charge current by means of the ISHE.

V. CONFIRMING THE FLOW OF SPIN CURRENT THROUGH THE BI LAYER

To confirm that the spin current is actually flowing through the Bi layer, we deposited an upper layer of W(6 nm) instead of the Pt layer. Fig. 4(a) and 4(b) show the SP
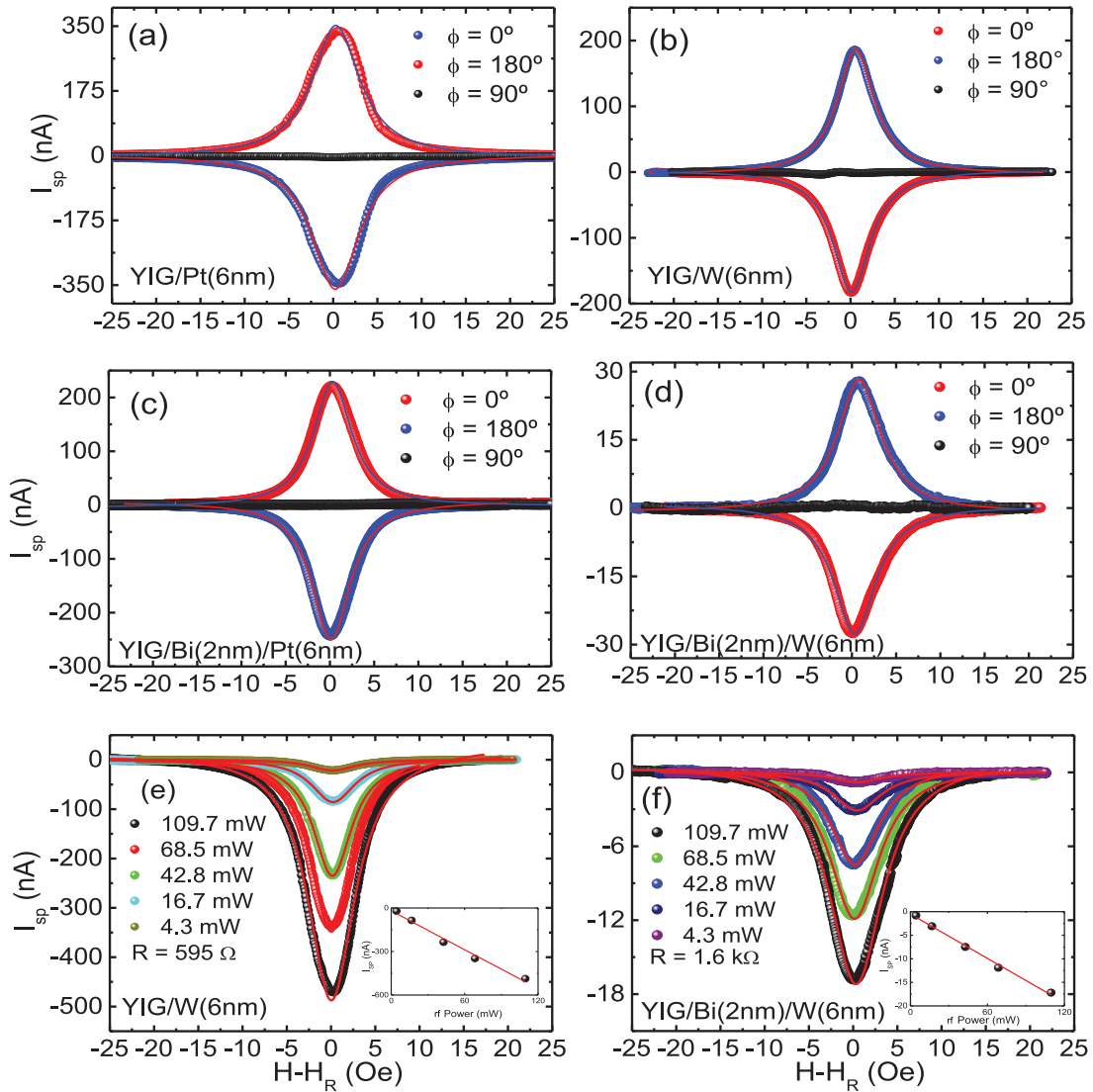
FIG. 4. Panels (a) and (b) show the SP signals generated by YIG/Pt(6 nm) and YIG/W(6 nm), respectively. Due to the opposite signals of the spin Hall angle of Pt and W, the polarizations are reversed. Panels (c) and (d) present the SP signals generated YIG/Bi(2 nm)/Pt(6 nm) and YIG/Bi(2 nm)/Pt(6 nm), respectively. These results confirm that the spin current flows through the Bi layer, being converted into charge current at the top layer of Pt [positive values, given by the red symbols in (c)] or at the top layer of W [negative values, given by the red symbols in (d)]. Panels (e) and (f) display the linear dependence of the SP signal as a function of the rf power.

current generated by the spin-charge current conversion measured in YIG/Pt(6 nm) and YIG/W(6 nm), respectively. As known, W has negative spin Hall angle in comparison to Pt [42,43], which is confirmed by the current signals displayed in Figs. 4(a) and 4(b), where $I_{SP}^{(Pt)}(\phi = 0°)$ is positive and $I_{SP}^{(W)}(\phi = 0°)$ is negative (red symbols), respectively. Figures 4(c) and 4(d) show the SP signal measured in YIG/Bi(2 nm)/Pt/(6 nm) and YIG/Bi(2 nm)/W(6 nm). As expected, the spin current flows through the Bi layer, reaching the W layer, as in the YIG/Bi(2 nm)/Pt(6 nm) structure, and being converted into a charge current with negative spin Hall angle. Figures 4(e) and 4(f) present the SP signal in YIG/W(6 nm) and YIG/Bi(2 nm)/W(6 nm), respectively, as a function of the incident rf power. The linear dependence of the SP signal indicates that the system is in the linear regime of excitation.

In conclusion, in this work we have unraveled the long-standing problem of converting spin-to-charge in bismuth using the SP technique. Contrary to some previous reports [18–20], we conclude that Bi, in spite of being the heaviest nonradioactive element with strong SOC, exhibits negligible spin-charge conversion. The SP voltage, which is generated in YIG/Bi bilayers under the FMR condition, cannot be explained by the equation $j_C = (2e/\hbar)\theta_{SH}(j_S \times \sigma)$. We attribute the anomalous signals shown in Figs. 1(c)–1(e) to the OSE, which is generated by the small ∇T in the plane of Bi films due to slight heating of the YIG film under the FMR condition. We have also added a top layer of Pt or W to the YIG/Bi bilayer and verified that the spin current flows through Bi without being converted into charge current, and then is injected into the top layer. In this case, the upper layer of Pt or W act as spin-to-charge current converters. We have also

found that the pumped spins relax to the lattice by means of a nontrivial relaxation mechanism, so that for the Bi layer thickness $t_{Bi} \approx 8$ nm there is essentially no spin current being injected into the top layer of Pt.

As Bi has the largest diamagnetic susceptibility among the elements [17], we propose a relaxation mechanism based on the exchange interaction between the pumped spins and the diamagnetic response of Bi to the applied magnetic field. Surprisingly, the heterostructure of YIG/Bi, in which a spin accumulation is pumped through the YIG/Bi interface, acts as a binary classification device, with the response function obeying the Fermi-Dirac distribution, as recently proposed in Ref. [40]. By adjusting the SP current measured at the top Pt layer as a function of t_{Bi} by Eq. (5), we were able to correlate the extracted effective parameters with intrinsic properties of the YIG/Bi device. We believe that the investigation reported here will open different perspectives involving fundamental aspects in the fields of machine learning [40,41] and condensed matter physics.

All data are included in the submitted material.

[1] W. Han, Y. Otani, and S. Maekawa, Quantum materials for spin and charge conversion, npj Quantum Mater. **3**, 27 (2018).

[2] F. Schindler, Z. Wang, M. G. Vergniory, A. M. Cook, A. Murani, S. Sengupta, A. Y. Kasumov, R. Deblock, S. Jeon, I. Drozdov, H. Bouchiat, S. Guéron, A. Yazdani, B. A. Bernevig, and T. Neupert, Higher-order topology in bismuth, Nat. Phys. **14**, 918 (2018).

[3] C.-H. Hsu, X. Zhou, T.-R. Chang, Q. Ma, N. Gedik, A. Bansil, S.-Y. Xu, H. Lin, and L. Fu, Topology on a new facet of bismuth, Proc. Natl. Acad. Sci. U.S.A. **116**, 13255 (2019).

[4] Y. Liu and R. E. Allen, Electronic structure of the semimetals Bi and Sb, Phys. Rev. B **52**, 1566 (1995).

[5] Di Yue, Weiwei Lin, and C. L. Chien, Negligible spin–charge conversion in Bi films and Bi/Ag(Cu) bilayers, APL Mater. **9**, 050904 (2021).

[6] M. Z. Hasan and C. L. Kane, Colloquium: Topological insulators, Rev. Mod. Phys. **82**, 3045 (2010).

[7] X.-L. Qi and S.-C. Zhang, Topological insulators and superconductors, Rev. Mod. Phys. **83**, 1057 (2011).

[8] J. Zhang, C.-Z. Chang, Z. Zhang, J. Wen, X. Feng, K. Li, M. Liu, K. He, L. Wang, X. Chen, Q.-K. Xue, X. Ma, and Y. Wang, Band structure engineering in $(Bi_{1-x}Sb_x)_2Te_3$ ternary topological insulators, Nat. Commun. **2**, 574. (2011).

[9] C. H. Li, O. M. J. van't Erve, J. T. Robinson, Y. Liu, L. Li, and B. T. Jonker, Electrical detection of charge-current-induced spin polarization due to spin-momentum locking in Bi_2Se_3, Nat. Nanotechnol. **9**, 218 (2014).

[10] A. R. Mellnik, J. S. Lee, A. Richardella, J. L. Grab, P. J. Mintun, M. H. Fischer, A. Vaezi, A. Manchon, E.-A. Kim, N. Samarth, and D. C. Ralph, Spin-transfer torque generated by a topological insulator, Nature (London) **511**, 449 (2014).

[11] J. B. S. Mendes, O. A. Santos, J. Holanda, R. P. Loreto, C. I. L. de Araujo, C.-Z. Chang, J. S. Moodera, A. Azevedo, and S. M. Rezende, Dirac-surface-state-dominated spin to charge current conversion in the topological insulator $(Bi_{0.22}Sb_{0.78})_2Te_3$ films at room temperature, Phys. Rev. B **96**, 180415(R) (2017).

[12] J. B. S. Mendes, M. Gamino, R. O. Cunha, J. E. Abrão, S. M. Rezende, and A. Azevedo, Unveiling the spin-to-charge current conversion signal in the topological insulator Bi_2Se_3 by means of spin pumping experiments, Phys. Rev. Mater. **5**, 024206 (2021).

[13] W. H. Campos, J. M. Fonseca, V. E. de Carvalho, J. B. S. Mendes, M. S. Rocha, and W. A. Moura-Melo, Topological insulator particles as optically induced oscillators: Toward dynamical force measurements and optical rheology, ACS Photonics **5**, 741 (2018).

[14] D. Zhang, M. Shi, T. Zhu, D. Xing, H. Zhang, and J. Wang, Topological Axion States in the Magnetic Insulator $MnBi_2Te_4$ with the Quantized Magnetoelectric Effect, Phys. Rev. Lett. **122**, 206401 (2019).

[15] M. M. Otrokov, I. I. Klimovskikh, H. Bentmann, D. Estyunin, A. Zeugner, Z. S. Aliev, S. Gaß, A. U. B. Wolter, A. V. Koroleva, A. M. Shikin, M. Blanco-Rey, M. Hoffmann, I. P. Rusinov, A. Y. Vyazovskaya, S. V. Eremeev, Y. M. Koroteev, V. M. Kuznetsov, F. Freyse, J. Sánchez-Barriga, I. R. Amiraslanov *et al.*, Prediction and observation of an antiferromagnetic topological insulator, Nature (London) **576**, 416 (2019).

[16] J. Li, Y. Li, S. Du, Z. Wang, B.-L. Gu, S.-C. Zhang, K. He, W. Duan, and Y. Xu, Intrinsic magnetic topological insulators in van der Waals layered $MnBi_2Te-$family materials, Sci. Adv. **5**, eaaw5685 (2019).

[17] Y. Fuseya, M. Ogata, and H. Fukuyama, Transport properties and diamagnetism of dirac electrons in bismuth, J. Phys. Soc. Jpn. **84**, 012001 (2015).

[18] D. Hou, Z. Qiu, K. Harii, Y. Kajiwara, K. Uchida, Y. Fujikawa, H. Nakayama, T. Yoshino, T. An, K. Ando, X. Jin, and E. Saitoh, Interface induced inverse spin Hall effect in Bismuth/permalloy bilayer, Appl. Phys. Lett. **101**, 042403 (2012).

[19] E. Emoto, Y. Ando, E. Shikoh, Y. Fuseya, T. Shinjo, and M. Shiraishi, Conversion of pure spin current to charge current in amorphous bismuth, J. Appl. Phys. **115**, 17C507 (2014).

[20] J. C. R. Sánchez, L. Vila, G. Desfonds, S. Gambarelli, J. P. Attané, J. M. De Teresa, C. Magén, and A. Fert, Spin-to-charge conversion using Rashba coupling at the interface between nonmagnetic materials, Nat. Commun. **4**, 2944 (2013).

[21] A. Tsukahara, Y. Ando, Y. Kitamura, H. Emoto, E. Shikoh, M. P. Delmo, T. Shinjo, and M. Shiraishi, Self-induced inverse spin

Hall effect in permalloy at room temperature, Phys. Rev. B **89**, 235317 (2014).

[22] A. Azevedo, R. O. Cunha, F. Estrada, O. Alves Santos, J. B. S. Mendes, L. H. Vilela-Leão, R. L. Rodríguez-Suárez, and S. M. Rezende, Electrical detection of ferromagnetic resonance in single layers of permalloy: Evidence of magnonic charge pumping, Phys. Rev. B **92**, 024402 (2015).

[23] S. Y. Huang, W. G. Wang, S. F. Lee, J. Kwo, and C. L. Chien, Intrinsic Spin-Dependent Thermal Transport, Phys. Rev. Lett. **107**, 216604 (2011).

[24] D. Xiao, Y. Yao, Z. Fang, and Q. Niu, Berry-phase Effect in Anomalous Thermoelectric Transport, Phys. Rev. Lett. **97**, 026603 (2006).

[25] R. Iguchi and E. Saitoh, Measurement of spin pumping voltage separated from extrinsic microwave effects, J. Phys. Soc. Jpn. **86**, 011003 (2017).

[26] S. Y. Huang, D. Qu, T. C. Chuang, C. C. Chiang, W. Lin, and C. L. Chien, Pure spin current phenomena, Appl. Phys. Lett. **117**, 190501 (2020).

[27] Y. Kajiwara, K. Harii, S. Takahashi, J. Ohe, K. Uchida, M. Mizuguchi, H. Umezawa, H. Kawai, K. Ando, K. Takanashi, S. Maekawa, and E. Saitoh, Transmission of electrical signals by spin-wave interconversion in a magnetic insulator, Nature (London) **464**, 262 (2010).

[28] See Supplemental Material at http://link.aps.org/supplemental/10.1103/PhysRevB.106.214418 for more details about the conditions employed for the preparation of samples and the crystallographic structure of YIG and Bi films.

[29] S. M. Rezende, *Fundamentals of Magnonics* (Springer, Berlin, 2020).

[30] K. Vandaele, S. J. Watzman, B. Flebus, A. Prakash, Y. Zheng, S. R. Boona, and J. P. Heremans, Thermal spin transport and energy conversion, Mater. Today Phys. **1**, 39 (2017).

[31] R. Gross and A. Marx, *Festkörperphysik* (Walter de Gruyter GmbH, Berlin, 2018).

[32] J. Cheng, K. He, M. Yang, Q. Liu, R. Yu, L. Sun, J. Ding, B. Miao, M. Wu, and H. F. Ding, Quantitative estimation of thermoelectric contributions in spin pumping signals through microwave photoresistance measurements, Phys. Rev. B **103**, 014415 (2021).

[33] P. Noël, M. Cosset-Cheneau, V. Haspot, V. Maurel, C. Lombard, M. Bibes, A. Barthelemy, Laurent Vila, and J.-P. Attané, Negligible thermal contributions to the spin pumping signal in ferromagnetic metal–platinum bilayers, J. Appl. Phys. **127**, 163907 (2020).

[34] K. Yamanoi, Y. Yokotani, and T. Kimura, Dynamical Spin Injection Based on Heating Effect Due to Ferromagnetic Resonance, Phys. Rev. Appl. **8**, 054031 (2017).

[35] T. Valet and A. Fert, Theory of the perpendicular magnetoresistance in magnetic multilayers, Phys. Rev. B **48**, 7099 (1993).

[36] S. Takahashi and S. Maekawa, Spin injection and detection in magnetic nanostructures, Phys. Rev. B **67**, 052409 (2003).

[37] F. Casanova, A. Sharoni, M. Erekhinsky, and I. K. Schuller, Control of spin injection by direct current in lateral spin valves, Phys. Rev. B **79**, 184415 (2009).

[38] N. G. Van Kampen, *Stochastic Processes in Physics and Chemistry* (Elsevier, Amsterdam, 2007).

[39] G. Kaniadakis, Generalized Boltzmann equation describing the dynamics of bosons and fermions, Phys. Lett. A **203**, 229 (1995).

[40] S.-C. Kim, A. S. Arun, M. E. Ahsen, R. Vogel, and G. Stolovitzky, The Fermi–Dirac distribution provides a calibrated probabilistic output for binary classifiers, Proc. Natl. Acad. Sci. U.S.A. **118**, e2100761118 (2021).

[41] T. Hastie, R. Tibshirani, and J. Friedman, *The Elements of Statistical Learning: Data Mining, Inference, and Prediction* (Springer, Berlin, 2009).

[42] Y. Yao and Z. Fang, Sign Changes of Intrinsic Spin Hall Effect in Semiconductors and Simple Metals: First-Principles Calculations, Phys. Rev Lett. **95**, 156601 (2005).

[43] C.-F. Pai, L. Liu, Y. Li, H. W. Tseng, D. C. Ralph, and R. A. Buhrman, Spin transfer torque devices utilizing the giant spin Hall effect of tungsten, Appl. Phys. Lett. **101**, 122404 (2012).